Multi-stability and polariton solitons in microcavity wires

G. Slavcheva,[1,*] A. V. Gorbach,[1] A. Pimenov,[2] A. G. Vladimirov,[2,3] and D. V. Skryabin[1]

[1] *Department of Physics, University of Bath, Bath, BA2 7AY, United Kingdom*

[2] *Weierstrass Institute, Mohrenstrasse 39, D-10117 Berlin, Germany*

[3] *Lobachevsky University of Nizhny Novgorod, Russia*

compiled: March 20, 2015

Nonlinear polaritons in microcavity wires are demonstrated to exhibit multi-stable behaviour and rich dynamics, including filamentation and soliton formation. We find that the multi-stability originates from co-existense of different transverse cavity modes. Modulational stability and conditions for multi-mode polariton solitons are studied. Soliton propagation in tilted, relative to the pump momentum, microcavity wires is demonstrated and a critical tilt angle for the soliton propagation is found.

Strong exciton-photon coupling in semiconductor microcavities leads to formation of half-light half-matter quasiparticles (polaritons) [1]. Owing to their excitonic component polaritons exhibit very strong and fast nonlinear optical response and weaker diffraction. These properties make microcavity polaritons an attractive platform for developing prototypes of opto-eletronic devices for processing of information. Effects and devices such as low threshold optical bistability [2], optical switches [3], optical transistors [4], diodes [5] and Mach-Zehnder interferometer [6] have been demonstrated with microcavity polaritons. Recently, dark [7, 8] and bright microcavity polariton solitons [9–11] have been reported theoretically and experimentally. Solitons in planar microcavities operating in non-polaritonic regimes have been previously studied in the context of optical information buffering and memory devices [12, 13]. Polaritonic regimes of operation can be useful in optimizing these devices for lower power consumption and more compact dimensions. Large-aperture planar devices cannot be used to predictably bend trajectory of a polaritonic pulse or to make polaritonic couplers, X and Y junctions and interferometers. Lateral confinement can effectively boost polariton-polariton interaction and reduce the number of polaritons required for nonlinear processes, allowing observation of quantum effects such as squeezing, phase transitions, polaritonic blockade and others [14]. Previous studies of 2D microcavity polariton solitons have shown that the diffraction in a transverse to the soliton velocity direction is balanced only in a very narrow range of parameters [15] and microcavity mirror patterning has been suggested for guided solitons [9]. Here we study microcavity wires, where polaritons are confined vertically through Bragg mirrors and laterally through the total internal reflection [16]. An alternative geometry for soliton applications is semiconductor waveguides guiding exclusively through the total internal-reflection and with quantum wells (QWs) embedded inside the substrate (see, e.g., [17]). The first studies of exciton-photon coupling in planar waveguides are given in [18]. Transition into the strong coupling regime [19] and polariton amplification have been reported only recently [20]. Despite being more difficult to fabricate, microcavity wires have an advantage of providing significant group velocity reduction and employing well established resonant or nonresonant pumping schemes for loss compensation.

Considering ongoing experimental research into microcavity wires, it becomes important to extend theoretical understanding of the nonlinear effects such as bistability, parametric generation and solitons using experimentally realistic geometries and conditions. In this Letter, we use an established dimensionless mean-field model for the photonic and excitonic components of microcavity polaritons, see, e.g. [7, 9, 10], whereby an effective transverse confinement potential is introduced:

$$\partial_t E - i\left(\partial_x^2+\partial_y^2\right)E + \left[\gamma_c - i\delta_c - i\Delta - iU(y)\right]E = i\Omega_R(y)\Psi + E_p e^{i\kappa x}\,, \quad (1)$$

$$\partial_t \Psi + \left(\gamma_e - i\delta_e - i\Delta\right)\Psi + i\left|\Psi\right|^2\Psi = i\Omega_R(y)E\,. \quad (2)$$

Here, E and Ψ are the averages of the photon and exciton creation or annihilation operators, the normalization is such that $(\omega_R/g)|E|^2$ and $(\omega_R/g)|\Psi|^2$ are the photon and exciton numbers per unit area, g is the strength of exciton-exciton interaction [10], ω_R is the Rabi frequency in a planar homogeneous cavity, time is measured in the units of $T = 1/\omega_R$. The microcavity wire geometry is schematically shown in Fig. 1(a). The unit length, $L = \sqrt{\hbar/(2m_c\omega_R)}$ [7, 9], is determined by the effective cavity photon mass m_c. The lateral confinement in the cavity plane (along y-axis) is described by an effective potential $U(y)$ in the photonic component and a

* Corresponding author: g.slavcheva@bath.ac.uk

spatially confined normalized coupling $\Omega_R(y)$:

$$U(y) = U_{bg}\left[1 - e^{-(2y/w)^8}\right] \ , \ \Omega_R(y) = e^{-(2y/w)^8} \ , (3)$$

where w is the dimensionless wire width. The super-Gaussian potential above is chosen to avoid numerical issues with discontinuities of a square potential and to realistically describe the etched wire lateral facets.

We assume that the CW pump with normalized amplitude E_p is linearly polarized along y-axis, so that it mainly couples to quasi-TE wire modes. We treat E and Ψ in Eqs. (1,2) as amplitudes of photonic and excitonic components in this particular mode. Nonlinear coupling to quasi-TM modes can be neglected due to the large TE-TM splitting. The pump is incident at an angle θ such that $\sin\theta = \kappa\lambda_p/(2\pi L)$, λ_p is the pump wavelength and κ is the momentum component along the wire. The parameters δ_c, δ_e and Δ are dimensionless detunings of the cavity resonant frequency, excitonic resonance, and pump frequency from a reference frequency $\hbar\omega_0 = 1.55$eV ($\lambda_0 = 800$nm), respectively. Cavity and exciton damping constants are set equal: $\gamma_c = \gamma_e = \gamma$.

Parameter values for ω_R, L and U_{bg} are obtained from fitting the free polariton dispersion in a realistic wire calculated by finite-element Maxwell solver (Comsol).We consider a 3μm-wide wire with a 400nm-thick cavity ($\epsilon_c = 9$) and Bragg mirrors, each containing 25 periods of low- and high-index layers ($\epsilon_l = 9$, $\epsilon_h = 12.25$) of thickness $L_l = \lambda_0/(4\sqrt{\epsilon_l})$ and $L_h = \lambda_0/(4\sqrt{\epsilon_h})$, respectively. The empty cavity resonance for the fundamental mode is at $\hbar\omega_c \approx 1.551$eV. We assume a single QW with large oscillator strength, equivalent to several QWs with low oscillator strength each. This is justified since the linear mode profile and dispersion do not change with the number of QWs added. The only role of the QW is to provide the required Rabi splitting. The QW is modelled by a 15nm-thick layer with linear permittivity:

$$\epsilon_{qw} = \epsilon_c + \frac{H\omega_e^2}{\omega^2 - \omega_e^2 - i2\Gamma_e\omega_e} \ , \qquad (4)$$

where $\hbar\omega_e = 1.5505$eV, with ω_e - the exciton resonance transition frequency, $H = 0.015$ is the normalised oscillator strength and $\hbar\Gamma_e$ is the exciton linewidth due to dephasing, assumed to be of the order of $0.1meV$ [10].

Photon-exciton coupling causes Rabi splitting of each of the modes into lower- and upper-polariton branches. Numerically computed dispersions for the first three lower polariton modes ($0L$, $1L$ and $2L$) and for the upper branch (OU) are shown in Fig. 1(b). For the chosen H the Rabi splitting in the fundamental mode is $2\hbar\omega_R \approx 11$meV at $\kappa = 0$, comparable to the one in planar cavities [10]. This gives scaling of time $T \approx 0.12$ps, $\delta_c = -0.191$ and $\delta_e = -0.1$. The free polariton dispersion from Eqs.(1,2) fits well the computed one by fixing $L = 0.53\mu$m and $U_{bg} = -1$ (solid curves in Fig. 1(b)).

Similar to a planar cavity, the lower polariton effective mass becomes negative for transverse momenta $\kappa/L \gtrsim 1.2\mu m^{-1}$. Hence, we expect to observe excitation

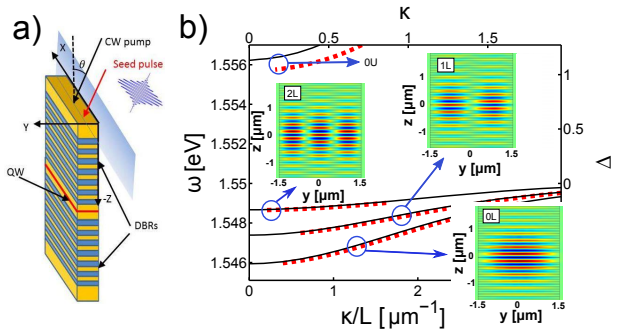

Fig. 1. (Color online) Microcavity wire: a) scheme of the geometry and excitation; b) Dispersion of free polaritons in the 3μm-wide wire: dashed lines correspond to data obtained from Comsol, solid lines - from model in Eqs. (1, 2). Insets show profiles of the dominant electric field component (E_y) of the first three quasi-TE cavity modes.

of bright solitons with large enough transverse (in-plane) momenta [10]. We choose $\kappa/L = 2.69\mu\text{m}^{-1}$ beyond the inflection points in all branches, yielding a pump incidence angle, $\theta \approx 20^\circ$ at $\lambda_p = 800$nm ($\Delta = 0$).

For a spatially homogeneous monochromatic pump, the stationary modes of Eqs. (1,2) are found using the ansatz $\{E, \Psi\} = \{A(y)\, e^{i\kappa x}, B(y)\, e^{i\kappa x}\}$. The resulting equations for A and B are solved numerically. In the zero pump and zero loss limit, $E_p = \gamma = 0$, we find that the nonlinear wire modes are continuously parameterized by the detuning Δ (dashed curves in Fig. 2(a)), and their number is increasing with Δ. For $E_p = const \neq 0$, each even mode ($OL, 2L, 4L, \dots$) exhibits a nonlinear resonance (solid curves in Fig. 2(a)). For pump frequencies above one or several branches of the polaritonic dispersion, microcavity wires' response can be either bistable or multi-stable, respectively. This is in contrast to planar homogeneous cavities, which are only bistable.

The microcavity wire modes, however, can be modulationally unstable, similar to the homogeneous solution in a planar cavity. To analyze this we add small perturbations to the modal profiles: $E = [A(y) + \epsilon_f(y)e^{iqx-i\delta t+\lambda t} + \epsilon_b^*(y)e^{-iqx+i\delta t+\lambda t}]e^{i\kappa x}$, $\Psi = [B(y) + p_f(y)e^{iqx-i\delta t+\lambda t} + p_b^*(y)e^{-iqx+i\delta t+\lambda t}]e^{i\kappa x}$ with q, δ, λ all real. The resulting eigenvalue problem:

$$(\delta + i\lambda)\vec{x} = \begin{bmatrix} -\mathcal{L}_f & 0 & -\Omega_R & 0 \\ 0 & \mathcal{L}_b^* & 0 & \Omega_R \\ -\Omega_R & 0 & -\mathcal{P} & B^2 \\ 0 & \Omega_R & -(B^*)^2 & \mathcal{P}^* \end{bmatrix} \vec{x} \ , \qquad (5)$$

$$\mathcal{L}_{f,b} = \partial_y^2 - (\kappa \pm q)^2 + \delta_c + \Delta + U + i\gamma_c,$$

$$\mathcal{P} = \delta_e + \Delta - 2|B|^2 + i\gamma_e \ , \ \vec{x} = [\epsilon_f, \epsilon_b, p_f, p_b]^T \ ,$$

is solved numerically.

In Figs. 2(b) and (c) stable, unstable (with $\lambda(q = 0) > 0$) and modulationally unstable ($\lambda > 0$ only for some $q \neq 0$) branches are plotted against pump amplitude E_p with solid black, dashed red/grey and solid red/grey curves, respectively, for different values of Δ and γ. For a pump frequency just above the lowest ($0L$)

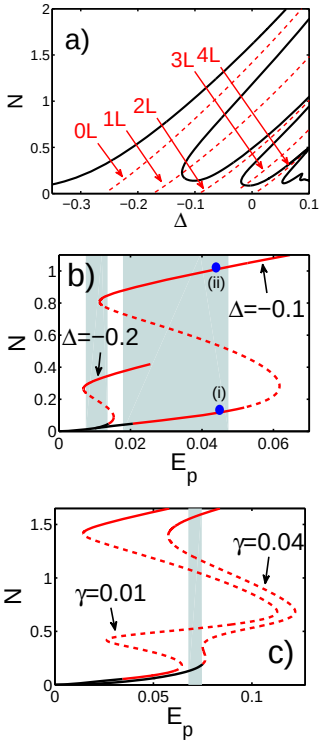

Fig. 2. (Color online) Stationary nonlinear modes (Ψ-norm $N = \int |\Psi|^2 dy$): (a) as function of the detuning Δ, $E_p = 0.005$, $\gamma = 0.01$. Dashed curves indicate families of nonlinear mode solutions $0L$-$4L$ in the limit $E_p = \gamma = 0$; (b) and (c) as functions of the pump amplitude E_p, $\Delta = -0.2$ and $\Delta = -0.1$, $\gamma = 0.01$ in (b), $\Delta = 0$, $\gamma = 0.01$ and $\gamma = 0.04$ in (c). Solid black, dashed red/grey and solid red/grey curves correspond to stable, unstable and modulationally unstable branches, respectively. Shaded areas in (b) and (c) indicate domains of existence of soliton solutions.

linear mode branch, $\Delta = -0.2$ cf. Fig. 2(a), the stationary microcavity wire mode is bistable within a range of E_p, see Fig. 2(b), where the lowest norm solution is stable, while the highest norm one is modulationally unstable. Similar behaviour is observed in planar cavities, where the co-existence of stable low-amplitude and modulationally unstable high-amplitude stationary modes is accompanied by the presence of bright solitons [9, 10].

We numerically found localized soliton solutions of Eqs. (1,2) of the form $\{E, \Psi\} = \{A_s(x - vt, y), B_s(x - vt, y)\}e^{i\kappa x}$, discretizing spatial coordinates and using Newton-Raphson iterations. Here the soliton velocity,v, is computed simultaneously with the soliton field profiles, A_s and B_s. For $\Delta = -0.2$ solitons exist within almost the entire domain of bistability of stationary modes, as shown by the shaded region in Fig. 2(b).

Increasing the pump frequency, the lowest norm stationary mode develops instabilities for E_p close to the turning point. The instability domain gradually expands with increasing pump frequency. For $\Delta = -0.1$, the mode is unstable within a large part of the entire bistability domain, see Fig. 2(b). In Fig. 3(a) the small perturbation gain λ is plotted against perturbation wave vector, q, for the mode at $E_p = 0.045$ [see marker (i) in Fig. 2(b)]. We found that the mode is modulationally unstable with respect to perturbations with different transverse profile, see insets in Fig. 3(a). The observed instabilities can be attributed to the co-existence of multiple transverse cavity modes in the wire potential. By contrast, the modulation instability of stationary modes from the highest norm branch is due to the perturbation with a transverse shape similar to the mode itself (Fig. 3(b)). To verify the linear stability analysis we solved Eqs. (1,2) perturbing solutions (i) and (ii). The evolved perturbed solutions exhibit filamentation and localised soliton-like features (Fig. 3(a,b):right panels).

For $\Delta = -0.1$ soliton solutions exist within a wide range of E_p (see corresponding shaded area of the bistability domain in Fig. 2(b)). However, having the homogeneous stationary mode from the lowest norm branch as their background, solitons share their stability properties with this mode. As a result, there is only a narrow window of E_p, where stable solitons can be excited.

As the pump frequency crosses a higher-order polaritonic branch ($2L$), additional branches of stationary mode solutions emerge (Figs. 2(a) and (c)). The instabilities of the lowest norm branch persist, affecting the existence and stability of solitons. For $\Delta = 0$ and $\gamma = 0.01$ we could not find stable soliton solutions, and all stationary modes are unstable within almost the entire domain of multi-stability (Fig. 2(c)). Increasing γ, the lowest branch can be stabilized, cf. plots for $\gamma = 0.01$ and $\gamma = 0.04$ in Fig. 2(c). For this higher value of γ we found stable soliton solutions (see shaded area in Fig. 2(c)).

To investigate dynamical formation of solitons within the range of bistability of stationary modes, we initialize the system with the stable mode from the lowest branch. The soliton is triggered by the writing pulse [10], which has duration of 2ps, intensity FWHM of 3μm (Gaussian beam) and the same momentum as the pump. An example of a soliton is shown in Fig. 4 for $\Delta = 0$ and $\gamma = 0.04$. The soliton is sitting on the lowest branch of stationary modes and extends to the highest branch in its core. The soliton pulse is squeezed along the wire and its temporal width of $T_p = 0.727$ps is nearly a half of that in a planar microcavity (~ 1.25ps [10]).

We found that solitons can be excited in wires tilted with respect to the pump momentum. Numerically exact soliton solutions, found with Newton-Raphson iterations,against waveguide tilt angle α, are plotted in Fig. 5. For fixed pump parameters, solitons persist within a finite interval of α, and the tilt can be as high as $\sim 10°$. Further studies of soliton properties and dynamics in microcavity wires will be reported elsewhere.

In summary, we investigated nonlinear polariton dynamics in microcavity wires within the modified mean-field model. The effective potential parameters are inferred from fitting the free polariton dispersion in a realistic geometry. We found that stationary excitations in microcavity wires exhibit multi-stable behaviour upon variation of pump parameters. This is a direct con-

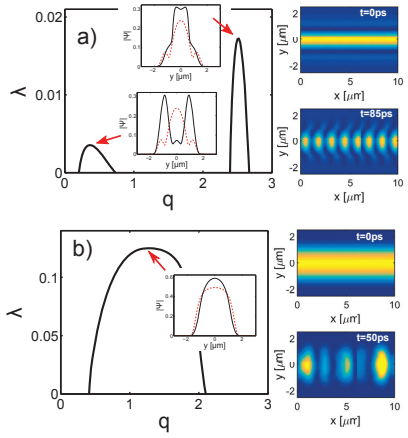

Fig. 3. (Color online) Perturbation growth rate of modulationally unstable modes for $\Delta = -0.1$, $E_p = 0.045$, $\gamma = 0.01$: lower branch (a) and upper branch (b), corresponding solutions are indicated as (i) and (ii) in Fig. 2(b). Insets show profiles (scaled) of unstable perturbations corresponding to local maxima of growth rate. Mode profiles are shown with dashed curves in insets. Right panels: modulation instability time evolution - filamentation (a) and localisation (b).

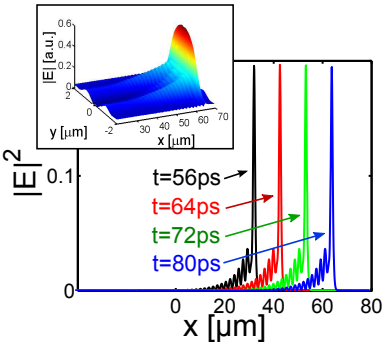

Fig. 4. (Color online) Dynamical soliton formation for $E_p = 0.075$, $\Delta = 0$, and $\gamma = 0.04$, the writing beam is applied at $t = 0$ps: insert - field snapshot at $t = 80$ps; field cross-sections throught the middle of the microcavity wire ($y = 0$) at different time instants.

sequence of the existence of different transverse cavity modes. Modulation instability and soliton formation in straight and tilted wires is discussed. Our results lay the foundations for further investigation of basic building blocks of polaritonic integrated circuits, such as $X-$ and $Y-$splitters, couplers, routers, based on soliton logic.

Funding through Leverhulme Trust Research Project Grant RPG-2012-481 and EU network project LIMACONA (Project No: 612600) is gratefully acknowledged. A.P. and A.G.V. acknowledge the support of SFB 787 of the DFG, project B5, and 14-41-00044 of RSF.

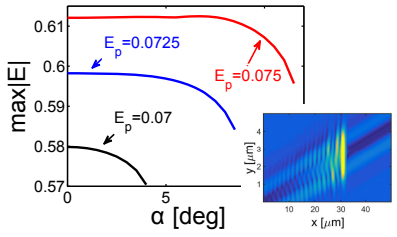

Fig. 5. (Color online) Soliton branches as functions of the microcavity wire tilt angle α for different amplitudes of the pump and $\Delta = 0$, $\gamma = 0.04$.

References

[1] A. Kavokin, J. Baumberg, G. Malpuech, and F. Laussy, *Microcavities* (Oxford University Press, Oxford, 2007).

[2] A. Baas, J. Karr, H. Eleuch, and E. Giacobino, Phys. Rev. A **69**, 023809 (2004).

[3] A. Amo, T. C. H. Liew, C. Adrados, R. Houdré, E. Giacobino, A. V. Kavokin, and A. Bramati, Nat. Photonics **4**, 361 (2010).

[4] T. Gao, P. S. Eldridge, T. C. H. Liew, S. I. Tsintzos, G. Stavrinidis, G. Deligeorgis, Z. Hatzopoulos, and P. G. Savvidis, Phys. Rev. B **85**, 235102 (2012).

[5] H. S. Nguyen, D. Vishnevsky, C. Sturm, D. Tanese, D. Solnyshkov, E. Galopin, A. Lemaître, I. Sagnes, A. Amo, G. Malpuech, and J. Bloch, Phys. Rev. Lett. **110**, 236601 (2013).

[6] C. Sturm, D. Tanese, H.S. Nguyen, H. Flayac, E. Galopin, A. Lemaître, I. Sagnes, D. Solnyshkov, A. Amo, G. Malpuech, and J. Bloch, Nat. Commun. **5**, 3278 (2014).

[7] A. V. Yulin, O. A. Egorov, F. Lederer, and D. V. Skryabin, Phys. Rev. A, **78**, 061801(R) (2008).

[8] A. Amo, T. C. H. Liew, C. Adrados, R. Houdré, E. Giacobino, A. V. Kavokin, and A. Bramati, Science **332**,11167 (2011)

[9] O. A. Egorov, D.V. Skryabin, A.V. Yulin, and F. Lederer, Phys. Rev. Lett. **102**, 153904 (2009).

[10] M. Sich, D. N. Krizhanovskii, M. S. Skolnick, A. V. Gorbach, R. Hartley, D. V. Skryabin, E. A. Cerda-Méndez, K. Biermann, R. Hey, and P. V. Santos, Nature Photonics, **6**, 50 (2012).

[11] M. Sich, F. Fras, J. K. Chana, M. S. Skolnick, and D. N. Krizhanovskii, Phys. Rev. Lett. **112**, 046403 (2014)

[12] S. Barland, J. R. Tredicce, M. Brambilla, L. A. Lugiato, S. Balle, M. Giudici, T. Maggipinto, L. Spinelli, G. Tissoni, T. Knödl, M. Miller, and R. Jäger, Nature **419**, 699 (2002).

[13] F. Pedaci, S. Barland, E. Caboche, P. Genevet, M. Giudici, J. R. Tredicce, T. Ackemann, A. J. Scroggie, W. J. Firth, G.-L. Oppo, G. Tissoni, and R. Jäger, Appl. Phys. Lett. **92**, 011101 (2008).

[14] I. Carusotto, and C. Ciuti, Rev. Mod. Phys. **85**, 299 (2013).

[15] O. A. Egorov, D.V. Skryabin, A.V. Yulin, and F. Lederer, Phys. Rev. Lett. **105**, 073903 (2010).

[16] E.Wertz, L. Ferrier, D. D. Solnyshkov, R. Johne, D. Sanvitto, A. Lemaître, I. Sagnes, R. Grousson, A. V. Kavokin, P. Senellart, G. Malpuech and J. Bloch, Nature Physics **6**, 860 (2010)

[17] N. Bêlanger, A. Villeneuve, and J. S. Aitchison, *J. Opt. Soc. Am. B* **14,** 3003 (1997).

[18] D. M. Beggs, M. A. Kaliteevski, S. Brand, R. A. Abram, V. V. Nikolaev, and A. V. Kavokin, J. Phys.: Condes. Matter **16**, 3410 (2004).

[19] P. M. Walker, L. Tinkler, M. Durska, D. M. Whittaker, I. J. Luxmoore, B. Royall, D. N. Krizhanovskii, M. S. Skolnick, I. Farrer, and D. A. Ritchie, Appl. Phys. Lett. **102**, 012109 (2013).

[20] D. D. Solnyshkov, H. Terças, and G. Malpuech, Appl. Phys. Lett. **105**, 231102 (2014).

References

[1] A. Kavokin, J. Baumberg, G. Malpuech, and F. Laussy, *Microcavities* (Oxford University Press, Oxford, 2007).

[2] A. Baas, J. Karr, H. Eleuch, and E. Giacobino, "Optical bistability in semiconductor microcavities", Phys. Rev. A **69**, 023809 (2004).

[3] A. Amo, T. C. H. Liew, C. Adrados, R. Houdré, E. Giacobino, A. V. Kavokin, and A. Bramati, "Exciton-polariton spin switches", Nat. Photonics **4**, 361 (2010).

[4] T. Gao, P. S. Eldridge, T. C. H. Liew, S. I. Tsintzos, G. Stavrinidis, G. Deligeorgis, Z. Hatzopoulos, and P. G. Savvidis,"Polariton condensate transistor switch", Phys. Rev. B **85**, 235102 (2012).

[5] H. S. Nguyen, D. Vishnevsky, C. Sturm, D. Tanese, D. Solnyshkov, E. Galopin, A. Lemaître, I. Sagnes, A. Amo, G. Malpuech, and J. Bloch,"Realization of a double-barrier resonant tunneling diode for cavity polaritons", Phys. Rev. Lett. **110**, 236601 (2013).

[6] C. Sturm, D. Tanese, H.S. Nguyen, H. Flayac, E. Galopin, A. Lemaître, I. Sagnes, D. Solnyshkov, A. Amo, G. Malpuech, and J. Bloch, "All-optical phase modulation in a cavity-polariton Mach-Zehnder interferometer", Nat. Communications **5**, 3278 (2014).

[7] A. V. Yulin, O. A. Egorov, F. Lederer, and D. V. Skryabin, "Dark polariton solitons in semiconductor microcavities," Phys. Rev. A, **78**, 061801(R) (2008).

[8] A. Amo, T. C. H. Liew, C. Adrados, R. Houdré, E. Giacobino, A. V. Kavokin, and A. Bramati,"Polariton superfluids reveal quantum hydrodynamic solitons," Science **332**,11167 (2011)

[9] O. A. Egorov, D.V. Skryabin, A.V. Yulin, and F. Lederer, "Bright Cavity Polariton Soliton," Phys. Rev. Lett. **102**, 153904 (2009).

[10] M. Sich, D. N. Krizhanovskii, M. S. Skolnick, A. V. Gorbach, R. Hartley, D. V. Skryabin, E. A. Cerda-Méndez, K. Biermann, R. Hey, and P. V. Santos, "Observation of bright polariton solitons in a semiconductor cavity," Nature Photonics, **6**, 50 (2012).

[11] M. Sich, F. Fras, J. K. Chana, M. S. Skolnick, and D. N. Krizhanovskii, "Effects of spin-dependent interactions on polarization of bright polariton solitons," Phys. Rev. Lett. **112**, 046403 (2014)

[12] S. Barland, J. R. Tredicce, M. Brambilla, L. A. Lugiato, S. Balle, M. Giudici, T. Maggipinto, L. Spinelli, G. Tissoni, T. Knödl, M. Miller, and R. Jäger, "Cavity solitons as pixels in semiconductor microcavities", Nature **419**, 699 (2002).

[13] F. Pedaci, S. Barland, E. Caboche, P. Genevet, M. Giudici, J. R. Tredicce, T. Ackemann, A. J. Scroggie, W. J. Firth, G.-L. Oppo, G. Tissoni, and R. Jäger, "All-optical delay line using semiconductor cavity solitons", Appl. Phys. Lett. **92**, 011101 (2008).

[14] I. Carusotto, and C. Ciuti, "Quantum fluids of light" Rev. Mod. Phys. **85**, 299 (2013).

[15] O. A. Egorov, D.V. Skryabin, A.V. Yulin, and F. Lederer, "Two-dimensional Localization of Exciton Polaritons in Microcavities," Phys. Rev. Lett. **105**, 073903 (2010).

[16] E.Wertz, L. Ferrier, D. D. Solnyshkov, R. Johne, D. Sanvitto, A. Lemaître, I. Sagnes, R. Grousson, A. V. Kavokin, P. Senellart, G. Malpuech and J. Bloch, "Spontaneous formation and optical manipulation of extended polariton condensates", Nature Physics **6**, 860 (2010)

[17] N. Bêlanger, A. Villeneuve, and J. S. Aitchison, "Solitonlike pulses in self-defocusing AlGaAs waveguides",*J. Opt. Soc. Am. B* **14,** 3003 (1997).

[18] D. M. Beggs, M. A. Kaliteevski, S. Brand, R. A. Abram, V. V. Nikolaev, and A. V. Kavokin, "Interaction of quantum well excitons with evanescent plane electromagnetic waves", J. Phys.: Condes. Matter **16**, 3410 (2004).

[19] P. M. Walker, L. Tinkler, M. Durska, D. M. Whittaker, I. J. Luxmoore, B. Royall, D. N. Krizhanovskii, M. S. Skolnick, I. Farrer, and D. A. Ritchie, "Exciton polaritons in semiconductor waveguides", Appl. Phys. Lett. **102**, 012109 (2013).

[20] D. D. Solnyshkov, H. Terças, and G. Malpuech, "Optical amplifier based on guided polaritons in GaN and ZnO", Appl. Phys. Lett. **105**, 231102 (2014).